JGR Space Physics

RESEARCH ARTICLE
10.1029/2025JA033778

Key Points:

- We investigate magnetic and flow shear effects on magnetopause reconnection from Magnetospheric Multiscale and Time History Events and Macroscale Interactions during Substorms observations
- The overall impact of magnetic shear ($B_g < 1$) is limited in active magnetopause reconnection events, whereas flow shear can induce significant X-line motion, particularly at the high-latitude magnetopause
- We propose a novel relationship that integrates the effects of both magnetic and flow shear

Correspondence to:
B. Tang and W. Li,
bbtang@spaceweather.ac.cn;
wyli@spaceweather.ac.cn

Citation:
Zhang, C., Tang, B., Li, W., Sang, L., Liu, H., Li, T., et al. (2025). Effects of magnetic shear and flow shear on magnetopause magnetic reconnection: Simultaneous observations from MMS and THEMIS. *Journal of Geophysical Research: Space Physics*, *130*, e2025JA033778. https://doi.org/10.1029/2025JA033778

Received 24 JAN 2025
Accepted 11 JUN 2025

Effects of Magnetic Shear and Flow Shear on Magnetopause Magnetic Reconnection: Simultaneous Observations From MMS and THEMIS

Chongle Zhang[1,2], Binbin Tang[1], Wenya Li[1], Longlong Sang[3,4], Huijie Liu[1,2], Tongkuai Li[1,2], Jiuqi Ma[4], Wenlong Guo[1,2], San Lu[4], Quanming Lu[4], and Chi Wang[1,2]

[1]Key Laboratory of Solar Activity and Space Weather, National Space Science Center, Chinese Academy of Sciences, Beijing, China, [2]College of Earth and Planetary Sciences, University of Chinese Academy of Sciences, Beijing, China, [3]Deep Space Exploration Laboratory, Institute of Deep Space Sciences, Hefei, China, [4]School of Earth and Space Sciences, University of Science and Technology of China, Hefei, China

Abstract Magnetic shear and flow shear form across Earth's magnetopause when shocked solar winds flow around Earth. Previous studies have shown that these two kinds of shears can similarly affect magnetopause reconnection. However, a direct investigation to evaluate their relative importance is lacking. In this study, we focus on simultaneous magnetopause reconnection observed by Magnetospheric Multiscale mission and Time History of Events and Macroscale Interactions during Substorms spacecraft at different magnetopause locations to quantitatively evaluate the magnetic shear and flow shear effects. The overall effect of magnetic shear (the normalized guide field < 1) is limited unless the guide field is sufficient strong to suppress reconnection, whereas the flow shear can significantly affect the observed reconnection outflow speed primarily by introducing non-zero X-line motion. Finally, we propose a novel relationship combining magnetic and flow shear effects by assuming independent X-line drift motion from these two effects, which shows that the X-line drift speed is dominated by the magnetosheath flow, and the suppression of reconnection is more likely to occur under strong guide field conditions. This study deepens our understanding on magnetopause reconnection occurrence and reconnection behaviors in large scales.

1. Introduction

Magnetic reconnection is a fundamental process that converts magnetic energy into plasma energy. In Earth space, magnetic reconnection occurs at the magnetopause (e.g., Sonnerup et al., 1981; Burch et al., 2016; Y. V. Khotyaintsev et al., 2016; Li et al., 2020), in the magnetotail (e.g., Nakamura et al., 2006; Torbert et al., 2018; Zhou et al., 2019), and in more turbulent environments such as the magnetosheath (e.g., Phan et al., 2018; Retinò et al., 2007). It serves as the primary driver of the Dungey cycle, and the dominant process for the solar wind energy entry into Earth's magnetosphere (Dungey, 1961). At the Earth's magnetopause, reconnection is usually asymmetric due to the significant differences in plasma and magnetic field parameters between the inflowing magnetosheath and magnetosphere region. Cassak and Shay (2007) has performed a scaling law analysis to incorporate this asymmetry, and the estimated reconnection outflow speed is expressed as

$$v_{out} = c_{A,asym} \sim \sqrt{\frac{B_1 B_2}{\mu_0} \cdot \frac{B_1 + B_2}{\rho_1 B_2 + \rho_2 B_1}}, \quad (1)$$

where $c_{A,\mathrm{asym}}$, B and ρ are asymmetric reconnection outflow speed, reconnecting magnetic fields and densities in the inflow region (denoted with subscripts 1 and 2 for the magnetosheath and magnetosphere region, as shown in Figure 1). This equation has been extensively tested in previous studies (e.g., Cassak & Fuselier, 2016; Cassak & Shay, 2007; Malakit et al., 2010) and has been frequently applied in magnetopause reconnection studies (e.g., Walsh et al., 2014; S. Wang et al., 2015).

Despite its asymmetry, another crucial feature for magnetopause reconnection is its widespread occurrence at the magnetopause, spanning from the subsolar region to the flanks (Haaland et al., 2020; B. Tang et al., 2021; Petrinec et al., 2022). The estimated reconnection X-line extends from less than 1 R_E to more than 10 R_E (Dunlop et al., 2011; Phan et al., 2000; Zou et al., 2019). Consequently, the reconnection environment varies significantly

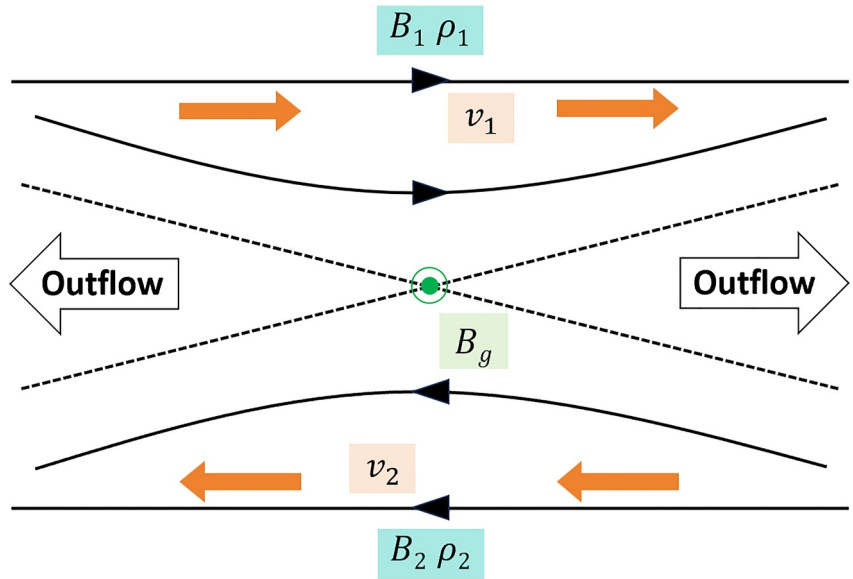

Figure 1. Sketch of magnetopause reconnection with the magnetic shear and flow shear (subscripts 1 and 2 denote the magnetosheath and magnetosphere). The magnetic shear (θ) is represented by the out-of-plane guide field (B_g). The plasma flow shear between the magnetosheath and magnetosphere is denoted by v_1 and v_2.

as the shocked solar wind compresses and flows around the Earth, leading to different degrees of asymmetry in the magnetopause reconnection at different regions. Meanwhile, it is noteworthy that the magnetic shear angle, formed by the magnetic fields in magnetosheath and Earth's magnetosphere, as well as the magnetosheath flow speed adjacent to the magnetopause reconnection site, can vary substantially across locations, potentially affecting the reconnection process.

When the magnetic shear angle (θ) is less than 180°, an out-of-plane component of the magnetic field, which is called the guide field (B_g, as shown in Figure 1) appears, increasing as θ decreases. The relationship between the magnetic shear angle and the normalized guide field in symmetric reconnection is given by $B_g = \tan\left(\frac{\theta}{2}\right)$. The guide field can affect reconnection in various ways, which can be associated with the asymmetric Hall structures, the enhanced parallel electric field, and the modulation of energy conversion (Wilder et al., 2018; Eastwood et al., 2018; B.-B. Tang et al., 2020; H.-W. Wang et al., 2023). Swisdak et al. (2003) shows that in the presence of the guide field (B_g), plasma experiences the diamagnetic drift parallel to the outflow, and the X-line is found to advect with the electrons, which is expressed as

$$v_{X-line,ms} = \frac{\nabla p_e \times \mathbf{B}_g}{q_e n B^2}, \tag{2}$$

where $v_{X-\mathrm{line,ms}}$, ∇p_e, q_e, n, and B are the X-line drift speed due to the magnetic shear (ms) effect, electron pressure gradient across the magnetopause, electron charge, plasma number density, and the total magnetic field strength, respectively. In the view of diamagnetic drifted ions, the X-line drift speed is the sum of the electron and ion diamagnetic drift speeds, which reduces the energy conversion efficiency from the magnetic field to plasma flows (Swisdak et al., 2003). The reconnection outflow speed in the X-line rest frame (XRF) can thus be expressed as

$$v_{out,ms}^{XRF} \sim \sqrt{c_{A,asym}^2 - \left(\frac{\nabla p \times \mathbf{B}_g}{|q_e| n B^2}\right)^2}. \tag{3}$$

where ∇p is the sum of the ion and electron pressure gradient across the magnetopause. Equation 3 shows how $v_{out,ms}^{XRF}$ decreases as B_g increases. When $v_{out,ms}^{XRF}$ reduces to ~ 0, reconnection is suppressed (Swisdak et al., 2003, 2010). This suppressed condition can also be approximately reformulated as $\Delta\beta > 2\frac{L_p}{d_i}\tan\left(\frac{\theta}{2}\right)$, where $\frac{L_p}{d_i}$ is the

normalized thickness of the reconnection current sheet. This condition is also known as the $\Delta\beta - \theta$ relationship, which has been statistically examined using reconnection data sets at the magnetopause (Phan et al., 2013; Trenchi et al., 2015), and has been applied to reconnection studies of different planetary magnetospheres (e.g., DiBraccio et al., 2013; Masters et al., 2012; Montgomery et al., 2022).

When the shocked solar wind flows around the magnetopause, it can have a component parallel to the reconnection outflows, introducing a flow shear at the two sides of inflow regions (denoted as v_1 and v_2 in Figure 1). Derived from the momentum equation, Doss et al. (2015) suggests that the X-line can drift due to this flow shear, which is quantified as

$$v_{X-line,fs} \sim \frac{\rho_1 B_2 v_1 + \rho_2 B_1 v_2}{\rho_1 B_2 + \rho_2 B_1}. \tag{4}$$

The subscript "fs" denotes the flow shear effect. Similarly, the reconnection outflow can be affected by the X-line drift motion, and the proposed outflow speed decreases as

$$v_{out,fs}^{XRF} \sim \sqrt{c_{A,asym}^2 - (v_1 - v_2)^2 \frac{\rho_1 B_2 \rho_2 B_1}{(\rho_1 B_2 + \rho_2 B_1)^2}}. \tag{5}$$

Reconnection is suppressed when $v_{out,fs}^{XRF} \sim 0$. At Earth's magnetopause, the flow shear is primarily caused by the magnetosheath flows and the magnetopause reconnection can be suppressed when the magnetosheath flow speed is about 20 times greater than $c_{A,\mathrm{asym}}$ under typical reconnection conditions (Doss et al., 2015). Recently, Sullivan et al. (2025) also shows that when the ratio of magnetosheath flow to Alfvénic speed reaches ~ 6.7 (without specifying the direction here), reconnection is not suppressed.

Both the magnetic shear (or B_g) and flow shear can cause X-line drift, reduce the reconnection outflow speed, and even suppress reconnection. At the magnetopause, these two shears can affect reconnection simultaneously, but which one is more important at various magnetopause regions is still an open question. To address this issue, we perform a comparative study to investigate the effects of magnetic shear and flow shear on reconnection using joint observations from the Magnetospheric Multiscale (MMS) mission and the Time History of Events and Macroscale Interactions during Substorms (THEMIS). Section 2 presents two events observed by MMS and THEMIS, which are used to quantitatively evaluate the independent effects of magnetic shear and flow shear in Section 3. In Section 4, we propose a new relationship combining these two shear effects. Finally, a brief summary is presented in Section 5.

2. Observations

We utilize data from the MMS and THEMIS to investigate magnetopause reconnection. The magnetic field and plasma parameters in MMS are obtained from the FluxGate Magnetometer (FGM; Russell et al., 2016) and the Fast Plasma Investigation instrument (FPI; Pollock et al., 2016), while the magnetic field and plasma parameters in THEMIS are from FGM (Auster et al., 2008) and the on-board calculated moments (MOM data product; McFadden et al., 2008). Due to small separations of MMS spacecraft, we primarily use MMS1 data in this study and for simplicity, only THEMIS-D (THD) data are presented.

To minimize the effect of time-varying upstream solar wind conditions, we require the nearly simultaneous magnetopause crossing from MMS and THEMIS (within 10 min) to search for possible reconnection events. From September 2015 to February 2023, we identify two such events. In these two events, MMS and THEMIS cross the subsolar, flank, and high-latitude magnetopause, respectively, due to their different orbit phases and orbit inclinations, allowing us to investigate the magnetic and flow shear effects on reconnection. We will first introduce these two events and perform the detailed analysis later.

2.1. Event on 13 January 2023

Figure 2 presents the simultaneous magnetopause crossing event of MMS and THD on 13 January 2023. In this event, MMS is located at the subsolar magnetopause ([10.30, 0.72, 0.90] R_E in GSM), while THD is at the dusk flank ([5.70, 11.80, 1.75] R_E). MMS and THD are located at two sides of the reconnection X-line, which can be

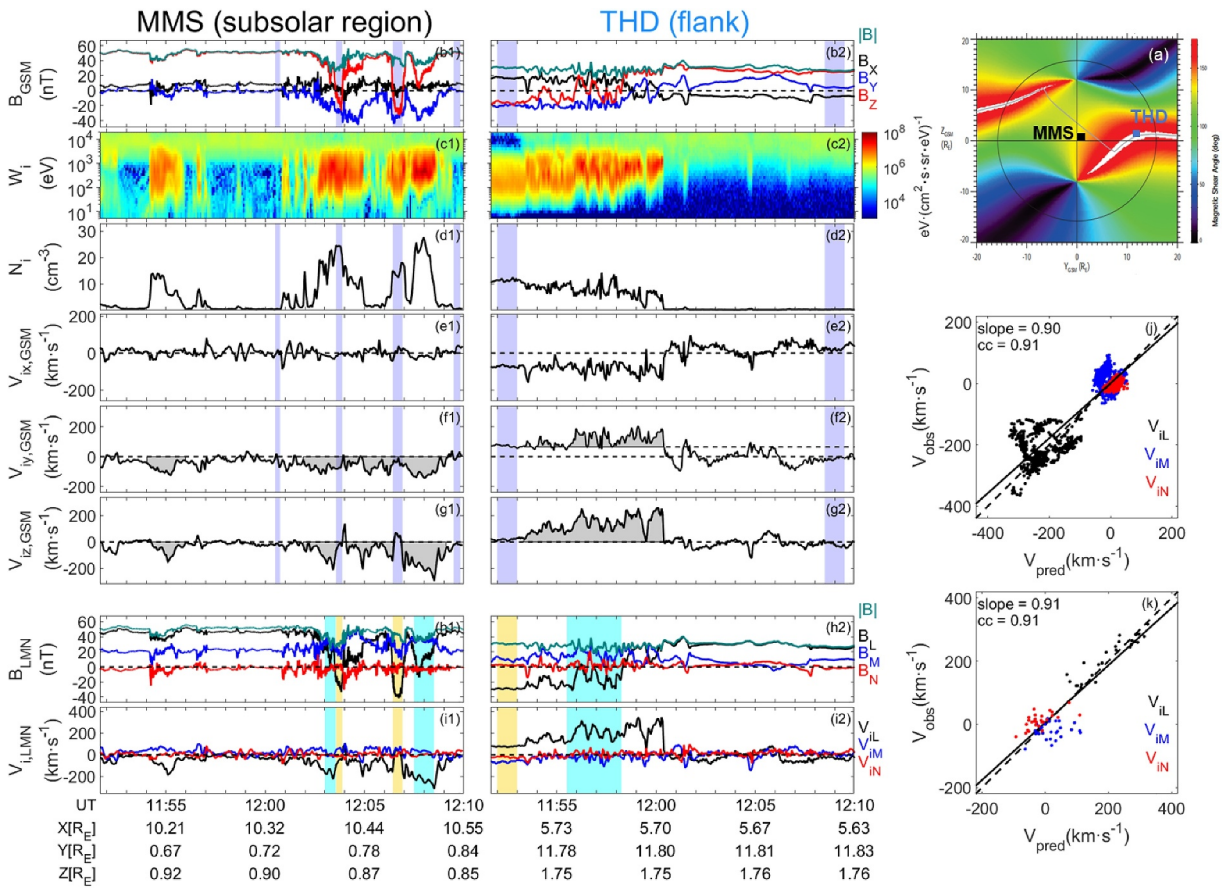

Figure 2. Overview of simultaneous magnetopause reconnection observed by Magnetospheric Multiscale (MMS) and THD on 13 January 2023. (a) The predicted X-line location (the gray line) at magnetopause from the Maximum Magnetic Shear Model (Trattner et al., 2007, 2021). The color shows magnetic shear angle across the magnetopause. MMS and THD are located at opposite sides of the X-line (shown by the black and blue squares). (b1–g1) MMS observations of the magnetic field, ion differential energy flux, ion number density, ion velocity in GSM. (h1–i1) MMS magnetic field and ion velocity in LMN ($\mathbf{L}$ = [0.11, 0.41, 0.90], $\mathbf{M}$ = [0.19, −0.90, 0.39], and $\mathbf{N}$ = [0.97, 0.13, −0.18]). (c2–i2) Similar to (c1–i1), but observed by THD (the local LMN: $\mathbf{L}$ = [−0.40, 0.49, 0.78], $\mathbf{M}$ = [0.36, −0.70. 0.62], and $\mathbf{N}$ = [0.84, 0.53, 0.10]). (j–k) Scatterplot of observed ion velocities versus the $\mathbf{V}_{pred}$ from MMS and THD.

predicted from the Maximum Magnetic Shear Model (Trattner et al., 2007, 2021) and is shown by the gray line in Figure 2a. Here, we obtain Figure 2a based on the following upstream solar wind parameters: $\mathbf{B}_{IMF}$ = [−2.0. −4.0, −4.0] nT and Psw = 1.1 nPa.

The overview of MMS observations is shown in Figures 2b1–2i1. MMS is initially in the magnetosphere, characterized by the northward B_z component (∼52 nT, Figure 2b1), high energy ions (>10^4 eV, Figure 2c1), and low ion density (<1 cm^{-3}, Figure 2d1). Then, MMS undergoes several magnetopause crossings, which is featured by a reversal of B_z (Figure 2b1), an increase of ion density (Figure 2d1) and an enhanced ion flow in the dawnward and southward direction (Figures 2f1 and 2g1). We note MMS has shortly entered into the magnetosheath (indicated by relatively low plasma speeds as shown by the purple-shaded time interval near 12:03 UT and 12:07 UT in Figures 2b1–2g1) before returning into magnetosphere. Then, we transform the observations into a local boundary-normal (LMN) coordinate system, which is determined by a hybrid variance analysis method (H.-W. Wang et al., 2023). First, the out-of-plane direction ($\mathbf{M}$) satisfies that $\mathbf{M} \parallel (\mathbf{B}_{msh} + \mathbf{B}_{msp}) \times (\mathbf{B}_{msh} - \mathbf{B}_{msp}) \times (\mathbf{B}_{msh} - \mathbf{B}_{msp})$, where $\mathbf{B}_{msh}$ and $\mathbf{B}_{msp}$ are the magnetosheath and magnetosphere magnetic field averaged over all their respective purple-shaded time intervals ($\mathbf{B}_{msh}$ = [1.3, −31.4, −18.3] nT and $\mathbf{B}_{msp}$ = [8.7, 0.4, 51.5] nT). The $\mathbf{L}'$ is along the maximum variance direction determined from the MVA method of the magnetic field from 12:00 UT to 12:10 UT, and $\mathbf{N} = \mathbf{L}' \times \mathbf{M}$. Finally, $\mathbf{L}$ completes the right-handed system ($\mathbf{L}$ = [0.11, 0.41, 0.90], $\mathbf{M}$ = [0.19, −0.90, 0.39], and $\mathbf{N}$ = [0.97, 0.13, −0.18]). The advantage of this hybrid method is that we can better evaluate B_M for latter analysis. In this LMN, we find a strong plasma flow of ∼330 km s^{-1} along the negative $\mathbf{L}$ direction (Figure 2i1). Then we perform the Walén test to check if it is a reconnection jet. Taking the averaged value of the two yellow-shaded

magnetosheath (Figures 2h1 and 2i1) as a reference with subscript "ref", we compare the predicted plasma flow $\mathbf{V}_{\rm pred}$ ($\mathbf{V}_{\rm pred} = \mathbf{V}_{\rm ref} \pm (\mu_0\rho_{\rm ref})^{-1/2}(\mathbf{B}_{\rm obs} - \mathbf{B}_{\rm ref})$, in which the plus/minus sign indicates that the plasma flow is aligned or anti-aligned with the local magnetic field, Paschmann et al., 1979) with observations in the cyan shaded region and show the scatter plot in Figure 2j. The results show that the velocity change across the boundary is roughly Alfvénic, indicating the tested boundary is a rotational discontinuity and the enhanced plasma flow is reconnection outflow.

THD crosses the magnetopause at the dusk flank nearly at same time (Figures 2b2–2i2). During this magnetopause crossing, THD observes a large plasma flow in the duskward and northward direction (Figures 2f2 and 2g2), which is in the opposite direction of that from MMS (Figures 2f1 and 2g1). In local LMN coordinates ($\mathbf{L} = [-0.40, 0.49, 0.78]$, $\mathbf{M} = [0.36, -0.70, 0.62]$, and $\mathbf{N} = [0.84, 0.53, 0.10]$), this enhanced plasma flow is well along the L direction (Figure 2j2) and the Walén test indicates it is a reconnection jet (Figure 2k).

Both MMS and THD observe clear magnetopause reconnection, and the reconnection flows are in opposite directions, consistent with the predictions shown in Figure 2a. We note reconnection parameters are significantly different at MMS and THD, that is the reconnecting $B_{\rm L}$ (Figures 2h1 and 2h2) and the plasma density (Figures 2d1 and 2d2), which are caused by the shocked solar wind when compressing and flowing around the Earth. Usually, we can use these reconnection parameters to evaluate the reconnection outflow with Equation 1, but the reconnection guide field and the flow shear are also significantly different: MMS observes a larger $B_{\rm M}$ (Figure 2h1), while THD records an obvious magnetosheath flow the in L direction (~77 km s^{-1}, Figure 2i2). Whether this guide field and flow shear can affect the reconnection outflow will be analyzed in detail in the next section.

2.2. Event on 17 April 2022

Figure 3 shows the other simultaneous magnetopause reconnection event observed by MMS and THD on 17 April 2022. In this event, the X-line locations can be predicted from the Maximum Magnetic Shear Model based on the following upstream solar wind parameters: $\mathbf{B}_{\rm IMF} = [-2.7, 6.1, -1.9]$ nT, $P_{\rm sw} = 1.4$ nPa (Figure 3a), and we find the predicted X-line orientation (Figure 3a) differs from that in Event 1 due to the sign change of IMF $B_{\rm y}$ component. MMS is located at the high-latitude magnetopause ([8.32, −2.48, −7.41] $R_{\rm E}$), while THD is at the dawn-side flank magnetopause ([5.57, −11.62, 0.07] $R_{\rm E}$). Both MMS and THD observe clear reconnection jets during magnetopause crossings and they are located at two sides of the reconnection X-line from the directions of reconnection jets (Figures 3f1–3g1 and 3f2–3g2). At the high-latitude magnetopause, MMS observes a large magnetosheath flow in the reconnecting L direction (~187 km s^{-1}, Figure 3i1), providing a good opportunity to investigate the flow shear effect on reconnection.

3. Evaluation of the Magnetic and Flow Shear Effects

To quantify the effects of magnetic shear and flow shear on reconnection, we list the reconnection parameters of the two events above in Table 1. These parameters are given by the mean values of the purple-shaded regions in Figures 2 and 3. Although these numbers are presented with uncertainties, which can be relatively large as a result of unsteady reconnection environments, there are some further discrepancies in determining these parameters as the spacecraft are not co-located with the reconnection X-line. These discrepancies are not included in this study since the reconnection parameters differ significantly due to large separations between MMS and THEMIS (>10 $R_{\rm E}$). A more careful approach is to search reconnection events including flow reversals to ensure spacecraft are close to the reconnection X-line (Trenchi et al., 2015).

From Table 1, the asymmetry of magnetic field and plasma density differs between MMS and THD in these two events due to the compression effect of the shocked solar wind, and the most pronounced asymmetry is recorded at the subsolar region. The magnetic shear angles (θ) are approximately in the range of 110°–140°, corresponding to a guide field of 10–20 nT (the normalized guide field $\frac{B_g}{\sqrt{B_1 B_2}}$ varies between 0.35 and 0.65). This indicates a moderate guide field here. While the flow shear exhibits significant variations at different locations. At the subsolar region, the magnetosheath flow is very weak (~20 km s^{-1}, as shown in Table 1). The magnetosheath flows are then accelerated at the flank and high latitude magnetopause. However, the magnetosheath flow at flanks may have a component in the out-of-plane direction, and the most significant magnetosheath flow (~187 km s^{-1}) is observed by MMS at the high-latitude region in Event 2.

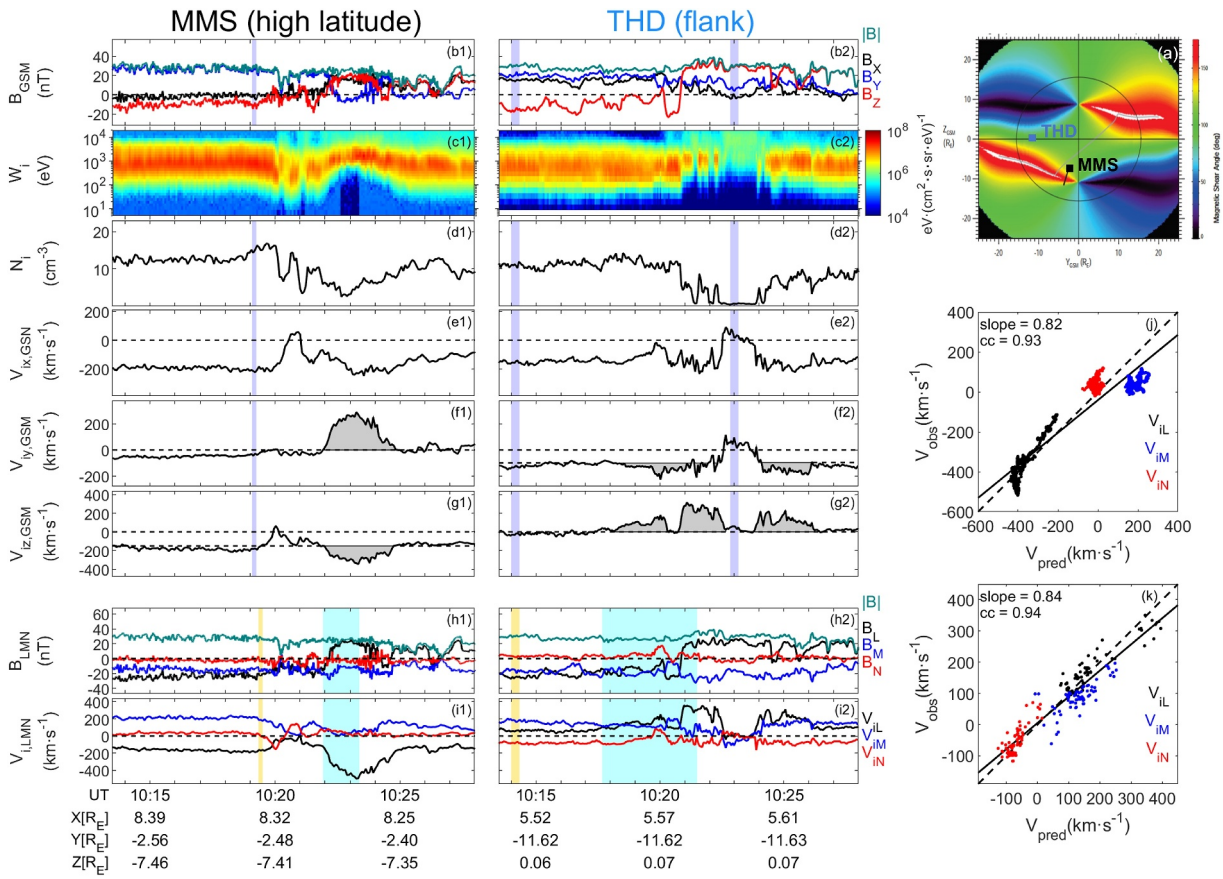

Figure 3. Overview of simultaneous magnetopause reconnection observed by Magnetospheric Multiscale (MMS) and THD on 17 April 2022. The figure format is similar to that in Figure 2. The LMN coordinates are **L** = [0.44, −0.65, 0.62], **M** = [−0.63, −0.71, −0.31], and **N** = [0.64, −0.26, −0.72] for MMS, and **L** = [−0.25, −0.34, 0.91], **M** = [−0.38, −0.83, −0.41], and **N** = [0.90, −0.45, 0.08] for THD.

With these reconnection parameters, we can estimate the ideal reconnection outflow speed from Equation 1, shown by the leftmost bar in each panel of Figure 4 for Event 1 and Event 2. These predictions are different from observations (indicated by the black dashed lines), and the difference could reach to ∼200 km s^{-1}. Then, we analyze whether the effects of magnetic and flow shears can explain these differences. The magnetic and flow shears can affect reconnection outflow speed in two ways: (a) they can decrease the reconnection outflow speed directly (denoted by the red rectangle of the middle and rightmost bar) and (b) the observed outflow is recorded in the spacecraft frame, which is different from the predictions in Equations 3 and 5 in the XRF due to the non-zero X-line drift motion, and we should transfer these predictions to the spacecraft frame (denoted by the blue diagonal-striped rectangle) to compare with observations.

In Event 1, the normalized guide field at the subsolar region is about 0.54, which results into a reduction of the outflow speed by ∼7 km s^{-1}, and a drift speed of X-line at ∼18 km s^{-1}. So the overall effect of the magnetic shear is not significant (the middle bar in Figure 4a). The flow shear effect is also very limited and the weak magnetosheath flow only contributes to a drift motion of X-line at ∼14 km s^{-1}. This means both the magnetic and flow shears can account for the differences between observations and predictions on the order of ∼10 km s^{-1}. In the flank region, the magnetic shear effect is similar to that at the subsolar region (Figure 4b). The enhanced magnetosheath flow leads to a X-line drift motion reaching about 74 km s^{-1}, making the prediction is more consistent with observations.

In Event 2, MMS is located at high-latitude magnetopause. It records a moderate guide field (∼0.57), whose overall effect is limited, and the most significant magnetosheath flow, which results into a large X-line drift speed (∼171 km s^{-1}) along the same direction with outflows (its reduction to the outflow speed is only ∼8 km s^{-1}).

Table 1
The Reconnection Parameters in Events 1 and 2, Which Are Estimated From the Mean Values Within the Purple-Shaded Intervals in Figures 2 and 3

	Event 1		Event 2	
S/C	MMS	THD	MMS	THD
Location (R_E, GSM)	[10.30, 0.72, 0.90]	[5.70, 11.80, 1.75]	[8.32, −2.48, −7.41]	[5.57, −11.62, 0.07]
$\mathbf{B}_{msh,LMN}$ (nT)[a]	[−29.39, 21.41, 0.50] ± [7.85, 5.28, 3.12]	[−28.93, 9.63, 2.25] ± [0.66, 1.97, 0.49]	[−25.57, −13.95, −0.12] ± [1.58, 0.82, 2.18]	[−24.83, −16.18, 2.61] ± [0.97, 2.14, 0.78]
$\mathbf{B}_{msp,LMN}$ (nT)[a]	[47.67, 21.41, −0.82] ± [1.21, 1.08, 0.97]	[24.71, 9.63, −1.92] ± [0.51, 0.48, 0.56]	[23.44, −13.95, 0.11] ± [0.07, 0.24, 0.10]	[25.14, −16.18, −2.65] ± [1.04, 1.15, 2.34]
n_1 (cm^{-3})	18.18 ± 5.11	11.43 ± 0.49	14.74 ± 0.74	11.05 ± 0.55
n_2 (cm^{-3})	0.40 ± 0.14	0.25 ± 0.02	1.12 ± 0.07	0.65 ± 0.09
ΔP (nPa)	0.63 ± 0.21	0.06 ± 0.01	0.37 ± 0.03	0.20 ± 0.04
θ (°)	∼120	∼140	∼121	∼114
B_g (nT)	21.41 ± 3.97	9.63 ± 1.41	13.95 ± 0.60	16.18 ± 1.64
$\frac{B_g}{\sqrt{B_1 B_2}}$	0.54 ± 0.11	0.36 ± 0.05	0.57 ± 0.02	0.65 ± 0.07
v_1 (km s^{-1})	−14 ± 49	77 ± 3	−187 ± 7	54 ± 5
v_2 (km s^{-1})	−24 ± 29	−30 ± 8	23 ± 9	10 ± 9

Note. In the table, $\mathbf{B}_{msh,LMN}$ and $\mathbf{B}_{msp,LMN}$ are magnetic field in the inflowing magnetosheath and magnetosphere region, n is the ion density, ΔP is the plasma pressure change across the magnetopause, θ is the magnetic shear angle between the magnetosheath and magnetosphere, B_g is the guide field strength, $\frac{B_g}{\sqrt{B_1 B_2}}$ is the normalized guide field, the plasma flows along the outflow direction in the magnetosheath and magnetosphere are denoted by v_1 and v_2. [a]The magnetic fields are presented in local LMN coordinate system.

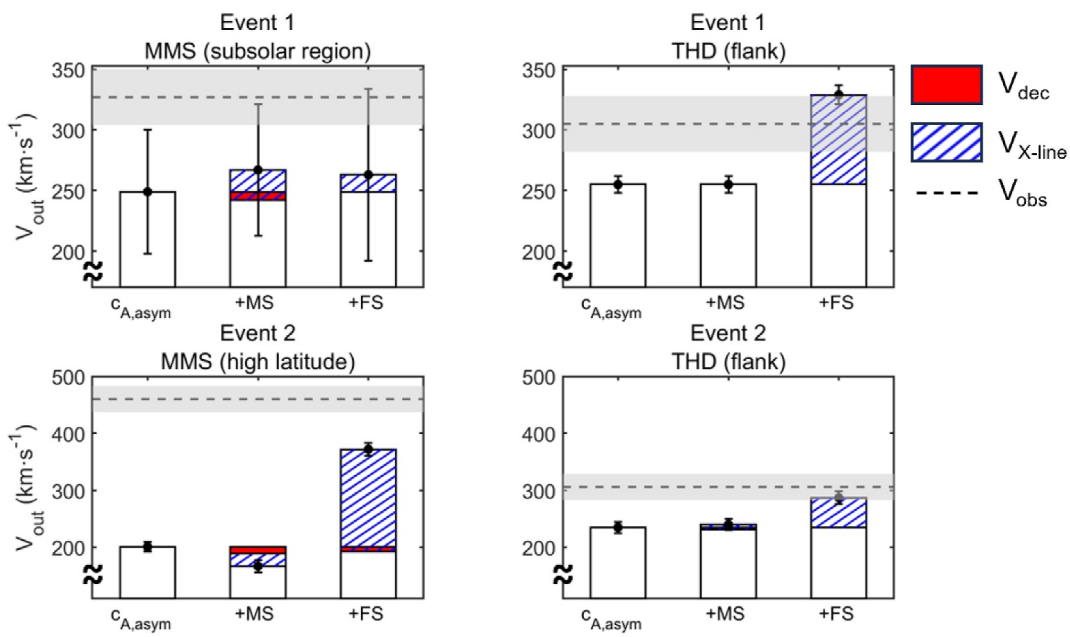

Figure 4. Histograms of the reconnection outflow speeds predicted under different conditions. In each panel, they are predictions from the Cassak-Shay equation (left), including magnetic shear effect (middle), and including the flow shear effect (right). When considering magnetic shear and flow shear effects, the decrease of the reconnection outflow speed is denoted by the red rectangle, and the X-line drift speed (denoted by the blue diagonal striped rectangle) indicates the transform from the X-line rest frame to the spacecraft frame. The black dashed line in each panel represents the observed outflow speed, which is determined by the mean value of the time interval exceeding 80% of the peak outflow speed, and the time interval with ion energy dispersion signatures is pre-excluded. The uncertainties of the outflow speeds are marked by the gray color.

Consequently, the predictions can better match observations. For THD at the flank region, the observed guide field and shear flow is similar to THD observations in Event 1, and their effects are similar as well.

Uncertainties of the reconnection parameters are also presented in Table 1, which lead to uncertainties of outflow speeds under different conditions. In Figure 4, such uncertainties are presented, while uncertainties from other sources are not considered. We find that the largest outflow uncertainties appear in the subsolar magnetopause reconnection observed by MMS in Event 1 (Figure 4a), and the errors are comparable to the difference between the observations and predictions. In Figures 4b–4d, the propagated uncertainties are relatively small.

Therefore, we conclude that the effect of a moderate guide field ($B_g < 1$) on reconnection is limited, as its contribution to the outflow speed reduction and the X-line drift motion is on the order of ∼10 km s^{-1}, which is negligible comparing to the predicted outflow speed. The guide field effect can be more important when its magnitude is close to the critical value to suppress reconnection. For example, the critical guide field is ∼1.76 for the parameters at the subsolar magnetopause in Event 1, which is stronger than the observed guide field in these two events. The flow shear can largely affect reconnection as it can lead into a large X-line motion speed, especially at high latitude magnetopause. Its effect on outflow reduction is much weaker in asymmetric magnetopause reconnection as suggested by Doss et al. (2015). In other words, the flow shears can affect magnetopause reconnection primarily by introducing non-zero X-line motion, which is the case in this study, but the magnitude of flow shear is usually not large enough to obviously reduce the outflow speed. As the guide field can vary in a wide range at magnetopause, its effect on reconnection is limited under moderate/weak guide field conditions, but reconnection can be suppressed when guide field is strong enough.

4. Discussion

In this study, we have investigated the magnetic shear and flow shear effects on magnetopause reconnection. Again, we note that the flow shear here is along the outflow direction, while the flow shear in the out-of-plane direction is also common in magnetopause reconnection. Previous studies have shown that flow shear can enhance the reconnection rate, distort the quadrupolar Hall field patterns, and increase the energy conversion rate (e.g., L. Wang et al., 2015). Under similar upstream flow shear conditions, the energy conversion rate is asymmetric at two sides of magnetospheric flanks (Liang et al., 2024). This flow shear effect in the out-of-plane direction is not considered in this study.

In Section 3, we focus on the individual effects of magnetic and flow shears on reconnection. However, the magnetic shear and flow shear do not occur independently at the magnetopause, which should have a combined effect on reconnection. Tanaka et al. (2010) has considered both the effects of magnetic shear and flow shear in the 2-D full-particle simulations, and shows that the X-line drift speed are dominantly by the magnetosheath flow for magnetopause reconnection. But how to function the outflow speed remains unclear. Based on previous studies to evaluate the magnetic and flow shear effects, the efficiency of the energy conversion in reconnection is affected by the X-line motion speed (Doss et al., 2015; Swisdak et al., 2003, 2010). So the key issue to combine these two effects is to estimate the X-line drift speed. Considering the X-line motion from the magnetic shear and flow shear are two independent processes, which can be evaluated from independent parameters, here we assume the combined X-line drift motion can be directly summed by these two shear effects, which is written as

$$v_{X-line} \sim v_{X-line,ms} \pm v_{X-line,fs}. \tag{6}$$

Then, following a similar way to subtract off the energy due to the combined effects (Equation A3 from Swisdak et al. (2010) and Equation 11 from Doss et al. (2015)), the reconnection outflow speed is expressed as

$$v_{out}^{XRF} \sim \sqrt{\begin{array}{l} c_{A,asym}^2 - \dfrac{\delta_{S1}}{2\delta}\left[v_1 - \left(v_{X-line,fs} \pm \dfrac{\nabla p \times \mathbf{B}_g}{qnB^2}\right)\right]^2 \\ \quad - \dfrac{\delta_{S2}}{2\delta}\left[v_2 - \left(v_{X-line,fs} \pm \dfrac{\nabla p \times \mathbf{B}_g}{qnB^2}\right)\right]^2 \end{array}}, \tag{7}$$

where δ_{S1} and δ_{S2} are the distance from the inflow (magnetosheath/magnetosphere) edges to the stagnation point, and $2\delta = \delta_{S1} + \delta_{S2}$. With some algebras, Equation 7 can be re-written as

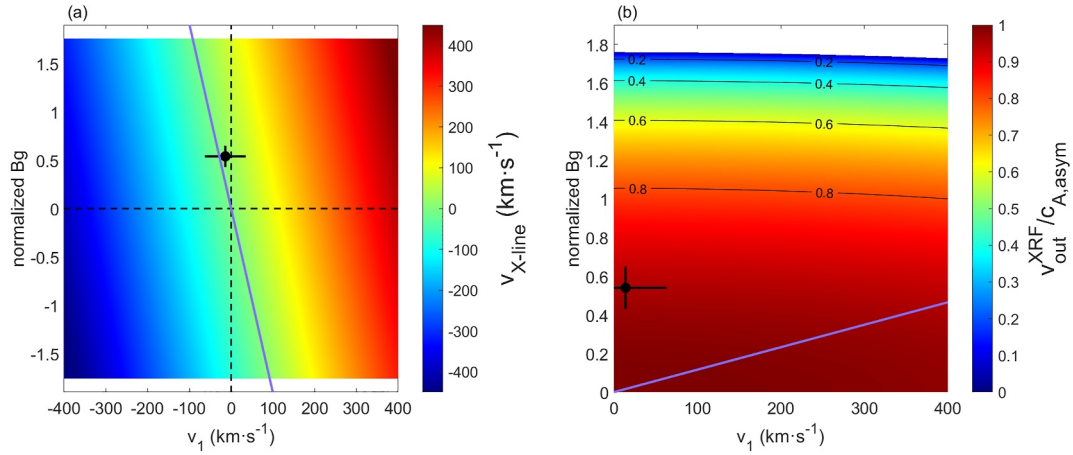

Figure 5. The combined magnetic and flow shear effects on the magnetopause reconnection with reconnection parameters at the subsolar magnetopause in Event 1 ($v_2 \sim 0$). (a–b) The X-line drift speed and the normalized reconnection outflow speed $\left(v_{out}^{XRF}/c_{A,asym}\right)$ as a function of magnetic shear (normalized guide field B_g) and magnetosheath flow. The black dots represent Magnetospheric Multiscale observations, and the purple lines show the condition when the magnetic shear and flow shear contribute equally to reconnection.

$$v_{out}^{XRF} \sim \sqrt{c_{A,asym}^2 - \left(\frac{\nabla p \times \mathbf{B}_g}{qnB^2}\right)^2 - (v_1 - v_2)^2 \frac{\rho_1 B_2 \rho_2 B_1}{\left(\rho_1 B_2 + \rho_2 B_1\right)^2}}. \quad (8)$$

This equation indicates the effects of magnetic shear and flow shear are decoupled, consistent with our assumption that these two shear effects are independent. In other words, we can consider their effects individually to get the combined effects on reconnection.

By substituting reconnection parameters at the subsolar magnetopause in Event 1 (we have set $v_2 \sim 0$) into Equations 6 and 8, we can obtain variations of the X-line drift speed and the reconnection outflow speed with normalized guide field and magnetosheath flows in the XRF (Figure 5). The black dots represent MMS observations, and the purple lines show the condition when the magnetic shear and flow shear contribute equally to reconnection. From Figure 5, we can find that the X-line drift speed is dominated by the magnetosheath flow speed (Figure 5a), and the suppression of reconnection is more likely to occur under strong guide field conditions (Figure 5b). These results are similar to that when we consider these effects independently, showing the magnetic shear and flow shear affect magnetopause reconnection in different ways. Finally, we note that the results in Figure 5 are estimated by assuming the flow shear and magnetic shear effects are independent with each other, which should be further tested.

5. Summary

In this study, we present two events simultaneously observed by MMS and THEMIS to evaluate the effects of magnetic and flow shears on magnetopause reconnection. Our results show that the magnetic shear effect is limited with a moderate guide field ($B_g < 1$), while flow shear can significantly affect the observed outflow speed primarily due to the fast X-line drift motion, particularly at the high-latitude magnetopause. We further propose a novel formula to combine the magnetic and flow shear effects by assuming these two effects independently affect reconnection. From both individual and combined shear effects, they affect reconnection in significantly different ways under usual magnetosheath conditions: the magnetosheath flows primarily affect the X-line drift speed and thus the observed outflow speed, and reconnection suppression is more likely to occur under strong guide field conditions. Here we note only two events that are simultaneously observed by MMS and THEMIS are presented, and the relation combining both the magnetic shear and flow shear should be further tested. Such investigations can be performed with single spacecraft observations in a statistical view (e.g., Sullivan et al., 2025) and/or with simulations.

Data Availability Statement

MMS data are available at the MMS Science Data Center (https://lasp.colorado.edu/mms/sdc/public/about/browse-wrapper/). THEMIS data and the solar wind data are available at NASA's Coordinated Data Analysis Web (CDAWeb, http://cdaweb.gsfc.nasa.gov/). Data analysis was performed using the IRFU-MATLAB analysis package (Y. Khotyaintsev et al., 2022).

Acknowledgments
We thank Dr. Trattner for providing plots from the Maximum Magnetic Shear Model. This research was funded by the National Science Foundation of China Grants (42122032, 42188101, and 42274211). B.B. T. was supported by the Youth Innovation Promotion Association of the Chinese Academy of Sciences.

References

Auster, H., Glassmeier, K., Magnes, W., Aydogar, O., Baumjohann, W., Constantinescu, D., et al. (2008). The THEMIS fluxgate magnetometer. *Space Science Reviews*, *141*, 235–264. https://doi.org/10.1007/978-0-387-89820-9_11

Burch, J., Torbert, R., Phan, T., Chen, L.-J., Moore, T., Ergun, R., et al. (2016). Electron-scale measurements of magnetic reconnection in space. *Science*, *352*(6290), aaf2939. https://doi.org/10.1126/science.aaf2939

Cassak, P., & Fuselier, S. (2016). Reconnection at Earth's dayside magnetopause. *Magnetic reconnection: Concepts and applications*, 213–276. https://doi.org/10.1007/978-3-319-26432-5_6

Cassak, P., & Shay, M. (2007). Scaling of asymmetric magnetic reconnection: General theory and collisional simulations. *Physics of Plasmas*, *14*(10), 102114. https://doi.org/10.1063/1.2795630

DiBraccio, G. A., Slavin, J. A., Boardsen, S. A., Anderson, B. J., Korth, H., Zurbuchen, T. H., et al. (2013). MESSENGER observations of magnetopause structure and dynamics at Mercury. *Journal of Geophysical Research: Space Physics*, *118*(3), 997–1008. https://doi.org/10.1002/jgra.50123

Doss, C., Komar, C., Cassak, P., Wilder, F., Eriksson, S., & Drake, J. (2015). Asymmetric magnetic reconnection with a flow shear and applications to the magnetopause. *Journal of Geophysical Research: Space Physics*, *120*(9), 7748–7763. https://doi.org/10.1002/2015ja021489

Dungey, J. W. (1961). Interplanetary magnetic field and the auroral zones. *Physical Review Letters*, *6*(2), 47–48. https://doi.org/10.1103/physrevlett.6.47

Dunlop, M. W., Zhang, Q.-H., Bogdanova, Y. V., Trattner, K. J., Pu, Z., Hasegawa, H., et al. (2011). Magnetopause reconnection across wide local time. *Annales Geophysicae*, *29*(9), 1683–1697. https://doi.org/10.5194/angeo-29-1683-2011

Eastwood, J., Mistry, R., Phan, T., Schwartz, S., Ergun, R., Drake, J., et al. (2018). Guide field reconnection: Exhaust structure and heating. *Geophysical Research Letters*, *45*(10), 4569–4577. https://doi.org/10.1029/2018gl077670

Haaland, S., Paschmann, G., Øieroset, M., Phan, T., Hasegawa, H., Fuselier, S., et al. (2020). Characteristics of the flank magnetopause: MMS results. *Journal of Geophysical Research: Space Physics*, *125*(3), e2019JA027623. https://doi.org/10.1029/2019ja027623

Khotyaintsev, Y., Vaivads, A., Johansson, E., Nilsson, T., Karlsson, J., Graham, D., & Lindberg, M. (2022). irfu/irfu-matlab: V1. 16.3 [software]. *Zenodo*. https://doi.org/10.5281/zenodo.11550091

Khotyaintsev, Y. V., Graham, D., Norgren, C., Eriksson, E., Li, W., Johlander, A., et al. (2016). Electron jet of asymmetric reconnection. *Geophysical Research Letters*, *43*(11), 5571–5580. https://doi.org/10.1002/2016gl069064

Li, W., Graham, D. B., Khotyaintsev, Y. V., Vaivads, A., André, M., Min, K., et al. (2020). Electron bernstein waves driven by electron crescents near the electron diffusion region. *Nature Communications*, *11*(1), 141. https://doi.org/10.1038/s41467-019-13920-w

Liang, H., Chen, L.-J., Bessho, N., & Ng, J. (2024). Impact of the out-of-plane flow shear on magnetic reconnection at the flanks of Earth's magnetopause. *Journal of Geophysical Research: Space Physics*, *129*(10), e2024JA033154. https://doi.org/10.1029/2024ja033154

Malakit, K., Shay, M., Cassak, P., & Bard, C. (2010). Scaling of asymmetric magnetic reconnection: Kinetic particle-in-cell simulations. *Journal of Geophysical Research*, *115*(A10), A10223. https://doi.org/10.1029/2010ja015452

Masters, A., Eastwood, J., Swisdak, M., Thomsen, M., Russell, C., Sergis, N., et al. (2012). The importance of plasma β conditions for magnetic reconnection at Saturn's magnetopause. *Geophysical Research Letters*, *39*(8), L08103. https://doi.org/10.1029/2012gl051372

McFadden, J., Carlson, C., Larson, D., Ludlam, M., Abiad, R., Elliott, B., et al. (2008). The THEMIS ESA plasma instrument and in-flight calibration. *Space Science Reviews*, *141*, 277–302. https://doi.org/10.1007/978-0-387-89820-9_13

Montgomery, J., Ebert, R., Clark, G., Fuselier, S., Allegrini, F., Bagenal, F., et al. (2022). Investigating the occurrence of magnetic reconnection at Jupiter's dawn magnetopause during the Juno era. *Geophysical Research Letters*, *49*(14), e2022GL099141. https://doi.org/10.1029/2022gl099141

Nakamura, R., Baumjohann, W., Asano, Y., Runov, A., Balogh, A., Owen, C., et al. (2006). Dynamics of thin current sheets associated with magnetotail reconnection. *Journal of Geophysical Research*, *111*(A11), A11206. https://doi.org/10.1029/2006ja011706

Paschmann, G., Sonnerup, B. Ö., Papamastorakis, I., Sckopke, N., Haerendel, G., Bame, S., et al. (1979). Plasma acceleration at the Earth's magnetopause: Evidence for reconnection. *Nature*, *282*(5736), 243–246. https://doi.org/10.1038/282243a0

Petrinec, S., Burch, J., Fuselier, S., Trattner, K., Giles, B., & Strangeway, R. (2022). On the occurrence of magnetic reconnection along the terrestrial magnetopause, using Magnetospheric Multiscale (MMS) observations in proximity to the reconnection site. *Journal of Geophysical Research: Space Physics*, *127*(6), e2021JA029669. https://doi.org/10.1029/2021ja029669

Phan, T., Eastwood, J. P., Shay, M., Drake, J., Sonnerup, B. Ö., Fujimoto, M., et al. (2018). Electron magnetic reconnection without ion coupling in Earth's turbulent magnetosheath. *Nature*, *557*(7704), 202–206. https://doi.org/10.1038/s41586-018-0091-5

Phan, T., Kistler, L., Klecker, B., Haerendel, G., Paschmann, G., Sonnerup, B. Ö., et al. (2000). Extended magnetic reconnection at the Earth's magnetopause from detection of bi-directional jets. *Nature*, *404*(6780), 848–850. https://doi.org/10.1038/35009050

Phan, T., Paschmann, G., Gosling, J., Oieroset, M., Fujimoto, M., Drake, J., & Angelopoulos, V. (2013). The dependence of magnetic reconnection on plasma β and magnetic shear: Evidence from magnetopause observations. *Geophysical Research Letters*, *40*(1), 11–16. https://doi.org/10.1029/2012gl054528

Pollock, C., Moore, T., Jacques, A., Burch, J., Gliese, U., Saito, Y., et al. (2016). Fast plasma investigation for Magnetospheric Multiscale. *Space Science Reviews*, *199*(1–4), 331–406. https://doi.org/10.1007/s11214-016-0245-4

Retinò, A., Sundkvist, D., Vaivads, A., Mozer, F., André, M., & Owen, C. (2007). In situ evidence of magnetic reconnection in turbulent plasma. *Nature Physics*, *3*(4), 235–238. https://doi.org/10.1038/nphys574

Russell, C., Anderson, B., Baumjohann, W., Bromund, K., Dearborn, D., Fischer, D., et al. (2016). The Magnetospheric Multiscale magnetometers. *Space Science Reviews*, *199*, 189–256. https://doi.org/10.1007/978-94-024-0861-4_8

Sonnerup, B. Ö., Paschmann, G., Papamastorakis, I., Sckopke, N., Haerendel, G., Bame, S., et al. (1981). Evidence for magnetic field reconnection at the Earth's magnetopause. *Journal of Geophysical Research*, *86*(A12), 10049–10067. https://doi.org/10.1029/ja086ia12p10049

Sullivan, K., Fuselier, S., Trattner, K., Petrinec, S., Burch, J., & Gershman, D. (2025). An investigation into far-flank magnetic reconnection at Earth's magnetopause. *Journal of Geophysical Research: Space Physics*, *130*(1), e2024JA032663. https://doi.org/10.1029/2024ja032663

Swisdak, M., Opher, M., Drake, J., & Bibi, F. A. (2010). The vector direction of the interstellar magnetic field outside the heliosphere. *The Astrophysical Journal*, *710*(2), 1769–1775. https://doi.org/10.1088/0004-637x/710/2/1769

Swisdak, M., Rogers, B., Drake, J., & Shay, M. (2003). Diamagnetic suppression of component magnetic reconnection at the magnetopause. *Journal of Geophysical Research*, *108*(A5), 1218. https://doi.org/10.1029/2002ja009726

Tanaka, K. G., Fujimoto, M., & Shinohara, I. (2010). Physics of magnetopause reconnection: A study of the combined effects of density asymmetry, velocity shear, and guide field. *International Journal of Geophysics*, *2010*(1), 17. https://doi.org/10.1155/2010/202583

Tang, B., Li, W., Wang, C., Khotyaintsev, Y. V., Graham, D. B., Zhang, Q.-H., et al. (2021). Secondary magnetic reconnection at Earth's flank magnetopause. *Frontiers in Astronomy and Space Sciences*, *8*, 740560. https://doi.org/10.3389/fspas.2021.740560

Tang, B.-B., Li, W., Le, A., Graham, D. B., Wu, Y.-F., Wang, C., et al. (2020). Electron mixing and isotropization in the exhaust of asymmetric magnetic reconnection with a guide field. *Geophysical Research Letters*, *47*(14), e2020GL087159. https://doi.org/10.1029/2020gl087159

Torbert, R., Burch, J., Phan, T., Hesse, M., Argall, M., Shuster, J., et al. (2018). Electron-scale dynamics of the diffusion region during symmetric magnetic reconnection in space. *Science*, *362*(6421), 1391–1395. https://doi.org/10.1126/science.aat2998

Trattner, K., Mulcock, J., Petrinec, S., & Fuselier, S. (2007). Probing the boundary between antiparallel and component reconnection during southward interplanetary magnetic field conditions. *Journal of Geophysical Research*, *112*(A8), A08210. https://doi.org/10.1029/2007ja012270

Trattner, K., Petrinec, S., & Fuselier, S. (2021). The location of magnetic reconnection at Earth's magnetopause. *Space Science Reviews*, *217*(3), 41. https://doi.org/10.1007/s11214-021-00817-8

Trenchi, L., Marcucci, M. F., & Fear, R. (2015). The effect of diamagnetic drift on motion of the dayside magnetopause reconnection line. *Geophysical Research Letters*, *42*(15), 6129–6136. https://doi.org/10.1002/2015gl065213

Walsh, B., Foster, J., Erickson, P., & Sibeck, D. (2014). Simultaneous ground-and space-based observations of the plasmaspheric plume and reconnection. *Science*, *343*(6175), 1122–1125. https://doi.org/10.1126/science.1247212

Wang, H.-W., Tang, B.-B., Li, W., Zhang, Y.-C., Graham, D. B., Khotyaintsev, Y. V., et al. (2023). Electron dynamics in the electron current sheet during strong guide-field reconnection. *Geophysical Research Letters*, *50*(10), e2023GL103046. https://doi.org/10.1029/2023gl103046

Wang, L., Wang, X.-G., Wang, X.-Q., & Liu, Y. (2015). Asymmetric magnetic reconnection with out-of-plane shear flows in a two dimensional hybrid model. *Physics of Plasmas*, *22*(5), 052110. https://doi.org/10.1063/1.4919965

Wang, S., Kistler, L. M., Mouikis, C. G., & Petrinec, S. M. (2015). Dependence of the dayside magnetopause reconnection rate on local conditions. *Journal of Geophysical Research: Space Physics*, *120*(8), 6386–6408. https://doi.org/10.1002/2015ja021524

Wilder, F., Ergun, R., Burch, J., Ahmadi, N., Eriksson, S., Phan, T., et al. (2018). The role of the parallel electric field in electron-scale dissipation at reconnecting currents in the magnetosheath. *Journal of Geophysical Research: Space Physics*, *123*(8), 6533–6547. https://doi.org/10.1029/2018ja025529

Zhou, M., Huang, J., Man, H., Deng, X., Zhong, Z., Russell, C., et al. (2019). Electron-scale vertical current sheets in a bursty bulk flow in the terrestrial magnetotail. *The Astrophysical Journal Letters*, *872*(2), L26. https://doi.org/10.3847/2041-8213/ab0424

Zou, Y., Walsh, B. M., Nishimura, Y., Angelopoulos, V., Ruohoniemi, J. M., McWilliams, K. A., & Nishitani, N. (2019). Local time extent of magnetopause reconnection using space–ground coordination. *Annales Geophysicae*, *37*(2), 215–234. https://doi.org/10.5194/angeo-37-215-2019